ARTICLE

Hollow Core−Porous Shell Structure Poly(acrylic acid) Nanogels with a Superhigh Capacity of Drug Loading

Ying Chen,[†] Xianchuang Zheng,[†] Hanqing Qian,[†] Zhiqing Mao,[†] Dan Ding,[†] and Xiqun Jiang*[,†,‡]

Laboratory of Mesoscopic Chemistry and Department of Polymer Science & Engineering, College of Chemistry & Chemical Engineering, and Jiangsu Provincial Laboratory for Nanotechnology, Nanjing University, Nanjing 210093, People's Republic of China

ABSTRACT Poly(acrylic acid) (PAA) nanogels with a hollow core−porous shell structure were prepared by the direct polymerization of an acrylic acid monomer in the presence of hydroxypropylcellulose (HPC) and a cross-linking agent, *N*,*N*-methylenebisacrylamide, followed by removal of HPC from the generated HPC−PAA nanoparticles in a basic environment. The properties of PAA nanogel were characterized by dynamic light scattering, FT-IR, transmission electron microscopy, and atomic force microscopy. It is found that the nanogels have a hollow core−porous shell structure. Protein, bovine serum albumin (BSA), and an antitumor agent, doxorubicin hydrochloride, were used as model drugs to investigate their loading abilities as versatile drug-delivery vehicles. The nanogel exhibits surprisingly high loading ability to both protein and small molecular drugs. For example, the maximum BSA loading capacity of PAA nanogel can reach as high as 800% (i.e., 1 mg of nanogel can load about 8.0 mg of BSA). This high loading capacity may be related with the hollow core−porous shell structure of PAA nanogels. PAA nanogels have also shown sustained drug release properties and can cross biological barriers to deliver loaded cargo inside cells. Considering the high stability of the materials, simple and mild preparation procedure, high loading capacity, sustained-release property, and ability to protect biological agents from denaturation, PAA nanogels should be promising drug-delivery carriers for drug-delivery systems.

KEYWORDS: poly(acrylic acid) • nanogels • pH-sensitive • high capacity • hollow • porous

INTRODUCTION

In the past decades, nanocarrier drug-delivery systems (DDSs) have developed rapidly and successfully in academic laboratories and pharmaceutical companies all over the world (1). Many current DDSs are making progress toward improving the biocompatibility and drug payload of nanocarriers, reducing in vivo toxicity, and increasing drug selectivity (2−4). Among the DDSs currently used, nanogels are very promising as versatile drug-delivery carriers because of their high stability and environmental response. Most of them are responsive to environmental changes such as ionic strength, pH, and temperature and favor the need to better control drug administration (5−7). So far, various nanogels have been synthesized and widely used as drug-delivery carriers, exhibiting environmentally triggered- and sustained-release drug-delivery performance (8, 9). However, the drug-loading capacity of nanogels is generally low, although high loading capacity is important to reducing the dose of the carrier and clinic practice. Hollow structure nanocarriers have been desirable to achieve high drug payload because of their large storage volume (10). Several approaches have been developed so far to fabricate hollow nanoparticles, such as the self-assembly of lipids or block copolymers, layer-by-layer assembly, a template technique, or ultrasonic fabrication (11−19). However, the loading capacities of these hollow nanoparticles have not been significantly enhanced as expected. To address this issue, one strategy is to synthesize hollow nanogels with mesopore channels penetrating from the shell to the hollow interior. Although hollow core−porous shell structure polymer particles with a micrometer scale prepared by a template-directed approach have been reported (20), the integration of a porous shell and a hollow core into one nanoparticulate system is very small.

Previously, our group successfully prepared hydroxypropylcellulose−poly(acrylic acid) (HPC−PAA) nanoparticles with a semi-interpenetrating polymer network structure by the direct polymerization of an acrylic acid (AA) monomer in the presence of HPC and a cross-linking agent, *N*,*N*-methylenebisacrylamide (MBAAm) (21). The HPC−PAA nanoparticles are composed of HPC as the exterior shell and a PAA−HPC complex with an interpolymer hydrogen bond as the interior core (22, 23). Because the interaction between HPC and cross-linked PAA is noncovalent, the HPC component can be stripped from the nanoparticles in a basic environment. Here, we focus on the removal of HPC from the HPC−PAA nanoparticles and the structure of the pure PAA nanogel left. This protocol is very similar to macromolecular imprinting, where the functional monomers are

* To whom correspondence should be addressed. E-mail: jiangx@nju.edu.cn.
Received for review August 8, 2010 and accepted November 2, 2010
† Laboratory of Mesoscopic Chemistry and Department of Polymer Science & Engineering, College of Chemistry & Chemical Engineering.
‡ Jiangsu Provincial Laboratory for Nanotechnology.
DOI: 10.1021/am100709d

Published on Web 11/16/2010

polymerized in the presence of a template, which is subsequently removed by washing and/or extraction after the polymerization (24). We demonstrated that a hollow structure was generated in the PAA nanogel after removal of HPC from the HPC−PAA nanoparticles. More importantly, we found that the PAA nanogel exhibited an extraordinarily high capacity of loading proteins and anticancer drugs. The maximum loading capacity of protein can reach as high as 8.0 mg/mg of nanogel, which is 10 times higher than that of common polymer carriers. The release properties of the nanogels were investigated, and a sustained-release characteristic of the drug from the nanogel was observed under physiological pH and NaCl concentrations.

EXPERIMENTAL SECTION

Materials. Hydroxypropylcellulose (HPC) was purchased from Alfa Aesar Chemical Co. (M_w = 100 kDa). Acrylic acid (AA; Shanghai Guanghua Chemical Co.) was distilled under reduced pressure in a nitrogen atmosphere. Ascorbic acid was purchased from Jiangsu Huakang Chemical Co. (Nanjing, China). *N*,*N*′-Methylenebisacrylamide (MBAAm) and Rhodamine B isothiocyanate (RBITC) were purchased from Sigma-Aldrich Chemical Co. Bovine serum albumin (BSA) (M_w, 66.7 kDa) was purchased from Bio Basic Inc. (BBI). Doxorubicin hydrochloride (Dox) was purchased from Shanghai Aladdin Reagent Co. A Bradford protein assay reagent, which consisted of Brilliant Blue G in phosphoric acid and methanol, was purchased from Sangon Reagent Co. (Shanghai). All other reagents were of analytical grade and were used without further purification.

Preparation of the PAA Nanogels. The PAA nanogels were prepared as follows: in a typical run, 0.2 g of HPC and 0.15 g of MBAAm cross-linker were dissolved in 50 mL of a 0.4% (w/v) AA aqueous solution. The solution was stirred at room temperature until it became clear. Then 5 g of a 2% ascorbic acid solution and 50 mg of a 30% hydrogen peroxide (H_2O_2) aqueous solution were added into the reaction system to initiate AA polymerization at room temperature. When the polymerization of AA reached a certain level, opalescent suspension occurred, indicating the formation of HPC−PAA nanoparticles. The reaction was allowed to proceed at room temperature for 1 h. Afterward, the pH of the resultant suspension was adjusted from 3 to around 6−8 using 0.1 M NaOH, and the resultant suspension was centrifugated at 15 000 rpm for 20 min. Finally, the sedimentation of the obtained PAA nanogel was redispersed into distilled water.

Preparation of Drug-Loaded PAA Nanogels. Drug (BSA or Dox) loading in the PAA nanogels was carried out by the incubation method. Briefly, the PAA nanogel suspension was mixed with a solution containing the drug at a predetermined concentration. The mixed solution was stirred gently overnight to allow BSA or Dox absorption on the nanogel to reach isothermal equilibrium.

Evaluation of Drug Entrapment. The loading efficiency and loading capacity of nanogels were determined by separating the nanogels from the aqueous medium containing free drug through centrifugation (10 000 rpm, 30 min). The amount of free BSA in the supernatant was measured by the Bradford method using a UV spectrometer at 595 nm (25). The amount of Dox was determined by using an absorbance at 490 nm based on a calibration curve. The drug loading efficiency (LE) and loading capacity (LC) of the nanogels were calculated as follows:

$$\text{LE}\,(\%) = 100\% \times (\text{total amount of drug-free drug})/\text{total amount of drug}$$

$$\text{LC}\,(\%) = 100\% \times (\text{total amount of drug-free drug})/\text{dry nanogel weight}$$

Drug Release in Phosphate-Buffered Saline (PBS). The release of the drug from the nanogels in PBS (pH = 4.0 and 7.0, ionic strength = 0.1 M) at 37 °C was evaluated by the dialysis method. A purified drug-loaded PAA nanogel solution with a known drug concentration was placed inside a dialysis bag (MWCO = 100 kDa for BSA and 10 kDa for Dox) and dialyzed against a PBS solution at 37 °C. The released drug outside of the dialysis bag was sampled at defined time periods and measured by using a UV spectrometer.

In Vitro Cytotoxicity. The cell viability of the PAA nanogels on the LoVo cell lines was evaluated by a MTT assay. LoVo cells (5000 cells/well) were cultured in RPMI 1640 containing 10% fetal bovine serum in a 96-well multiplate. One row of the 96-well plates was used as the control. Then, the cells were exposed to nanogels for 48 h, and a MTT solution was added. The cell viability was measured by the formazan absorbance formed at 570 nm.

Cell Uptake. BSA molecules were labeled using dye RBITC in advance (RBITC-BSA). BCG 823 cells were incubated with RBITC-BSA- and Dox-loaded nanogels in a humidified atmosphere of 5% CO_2 at 37 °C, respectively. After incubation for 4 h to allow the BCG 823 cells to internalize the nanogels, the noninternalized nanogels were removed through washing three times with a PBS solution. Cells were observed using laser confocal scanning microscopy (LCSM; Zeiss LSM 710, Germany) at an excitation wavelength of 543 nm.

Characterization Methods. Fourier transform infrared (FT-IR) spectra were measured on a Bruker IFS 66 V vacuum-type spectrometer. The PAA nanogel suspension was lyophilized to a dry powder, which was mixed with KBr and pressed to a disk for measurement.

The mean diameter and size distribution of the PAA nanogels were measured by dynamic light scattering (DLS) using a Brookhaven BI9000AT system (Brookhaven Instruments Corp., Holtsville, NY). The ζ potential of the sample was obtained with Zetaplus (Brookhaven Instruments Corp.). All DLS measurements were done with a laser wavelength of 658.0 nm and an incident angle of 90° at 25 °C. The concentration of each sample was adjusted as 0.01% (w/v) with filtered distilled water or in a 0.01 M NaCl solution in the case of ζ-potential examination. All analyses were triplicated, and the result was the average of three runs.

The morphology of the PAA nanogel was observed by transmission electron microscopy (TEM; JEOL TEM-100). The sample was dripped onto a nitrocellulose-covered copper grid at room temperature without staining. Atomic force microscopy (AFM; SPI3800, Seiko Instruments, Japan) was used to study the surface morphology of the nanogel in great detail. One drop of a properly diluted nanogel suspension was placed on the surface of a clean silicon wafer and dried under a nitrogen flow at room temperature. The AFM observation was performed with as 20 μm scanner in tapping mode.

The stability of the released BSA was determined by measuring circular dichroism (CD) spectra, which were recorded on a Jasco-715 spectropolarimeter (Jasco, Tokyo, Japan).

RESULT AND DISCUSSION

Characterization of the PAA Nanogels. The procedure to prepare a hollow core−porous shell structure PAA nanogel consists of two steps, as shown in Scheme 1. The HPC−PAA nanoparticles with semi-interpenetrating polymer network structures were first prepared by the direct polymerization of AA monomers in a HPC aqueous solution

Scheme 1. Schematic Illustration of the Formation of Porous Hollow PAA Nanogels

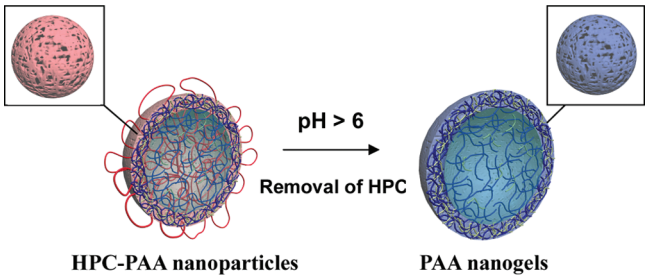

containing cross-linker MBAAm. Subsequently, as a result of dissociation of the interpolymer hydrogen bonds between PAA and HPC at a higher pH medium (pH > 6.0), HPC was removed from HPC−PAA nanoparticles and a hollow PAA nanogel was obtained because HPC mostly existed in the core of the particles (21). Figure 1 shows the FT-IR spectra of HPC−PAA nanoparticles, the PAA nanogels, and pure HPC. For HPC−PAA nanoparticles, the main absorption bands at 3438 cm^{-1} for the hydroxyl group, 1732 cm^{-1} for the carbonyl group of PAA, and 1070 cm^{-1} for the ether group of HPC are displayed. It can be seen that the relative intensity of a typical adsorption band for ether linkages of HPC at 1000−1100 cm^{-1} is much weaker for a HPC-stripped PAA nanogel, indicating that HPC is mostly removed from the HPC−PAA particles. The hydrodynamic diameter of a HPC-stripped PAA nanogel was determined to be about 230 nm by DLS, as shown in Figure 2. Compared to the original HPC−PAA particles, the size of the PAA nanogel increases by 80 nm, owing to stronger swelling and electrostatic repulsion generated by ionization of PAA at pH = 6.5. It is worth noting that PAA nanogels can be lyophilized without the need to add any cryoprotective agent, and the resultant dried powder is easy to redisperse in distilled water to a nanogel solution. The mean diameter of the nanogels after lyophilization and redispersion shows insignificant change compared to that of the original ones (Figure 2). This is very favorable for application in drug delivery.

When the PAA nanogels were incubated in buffer solutions with various pH values (ionic strength = 0.1M), the size and ζ potential of the nanogels decreased with a decrease of the pH value (Figure 3). When the pH value was larger than 5.7, the diameter of the nanogels were barely changed because of complete dissociation of the carboxyl groups in the PAA chain above this pH value. Likewise, no further condensation occurred below pH = 3.0 because of complete protonation of the carboxyl groups. This indicates that the PAA nanogels exhibit promising pH-responsive properties.

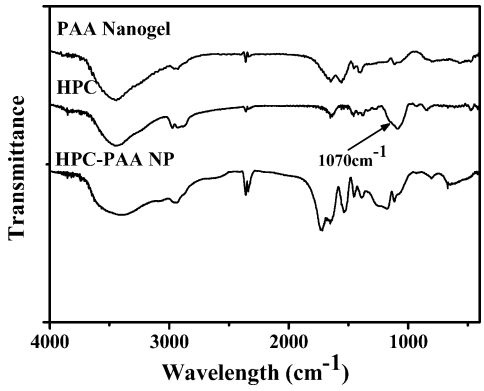

FIGURE 1. FT-IR spectra of HPC, HPC−PAA nanoparticles, and PAA nanogels.

Figure 4 displays the morphology and structure of the obtained PAA nanogels observed by AFM and TEM. For the AFM phase image, the bright regions correspond to the hard part and the dark regions correspond to the soft part. Thus, from the AFM phase image (Figure 4A), it can be seen that before HPC removal the HPC−PAA nanoparticles have a spherical shape with a solid structure and a porosity−structural shell. After removal of HPC, the PAA nanogels still maintain a spherical morphology but a hollow structure in the PAA nanogel interior is generated (Figure 4B). AFM height and phase images of the sample provide further evidence for the morphology of the obtained HPC-stripped PAA nanogels. As is seen from the height image in Figure 4C, the PAA nanogels appear as intact spheres with an average width of 101 nm, while in the phase image of Figure 4D, the bright spherical boundary and dark center region of the nanogels are observed. Apparently, the center of the PAA nanogel is very soft, which well corresponds to the hollow structure of the PAA nanogels. More interestingly, the mesopore channels penetrating from the shell to the hollow interior of the nanogels can be identified in the AFM phase image of the PAA nanogels (Figure 4D and inset). As discussed in our previous work (21), the HPC−PAA nanoparticles are semi-interpenetrating structures; the cross-linking degree of PAA in the nanoparticles decreased from the exterior shell to the interior core. Once HPC was stripped from the HPC−PAA nanoparticles, the surface density of the PAA nanogels must be greater than the middle for higher cross-linking. Therefore, the PAA nanogels displayed hollow structures under TEM observation. Probably, there are some light cross-linked PAA chains in the cavity of the PAA nanogels, which provide the drugs with supporting points to exist in the cavity.

Drug Loading of the PAA Nanogels. Because of the large cavity inside the hollow nanogel and the numerous mesopores presented in the shell, these PAA nanogels are expected to have promising application as high-loading drug carriers. Here, a BSA molecule, which is shaped as a prolate ellipsoid with major and minor axes of 13.8 and 4.6 nm (26), respectively, as a model protein, is loaded into the PAA nanogels. To maintain the activity of BSA, the drug loading was selected to be carried out by incubating the PAA nanogels with a BSA solution at room temperature. It was found that the PAA nanogels exhibit surprisingly high loading ability; that is, 1 mg of nanogel can load about 8.0 mg of BSA and the loading capacity reaches 800%. This capacity is 10 times larger than that of BSA in polysaccharide colloidal particles (27) and is over 50 times greater than that of BSA in micelles assembled by a block copolymer (28). From Table 1, it is found that the scattering light intensity of the BSA-loaded PAA nanogels was much higher than that of the PAA nanogel, while the size of the BSA-loaded PAA nanogels

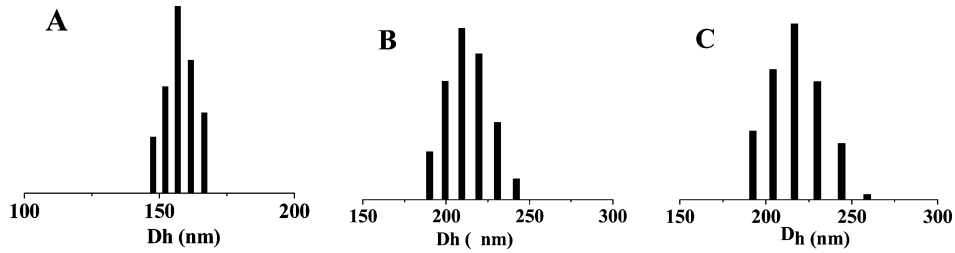

FIGURE 2. Hydrodynamic diameter distribution of (A) the HPC−PAA particles in an aqueous medium with pH = 3.1, (B) PAA nanogels in an aqueous medium with pH = 6.5, and (C) PAA nanogels after lyophilization and redispersion in an aqueous medium with pH = 6.5.

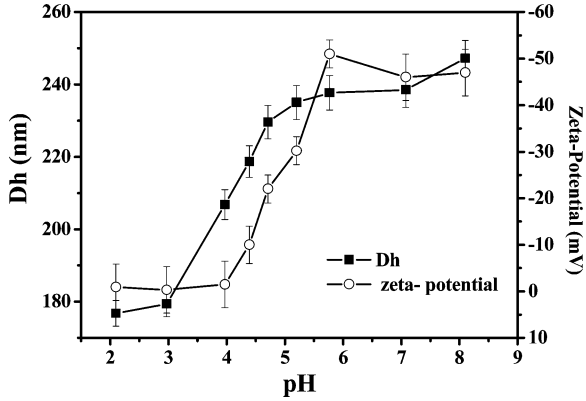

FIGURE 3. Size and ζ potential of PAA nanogels at different pH values.

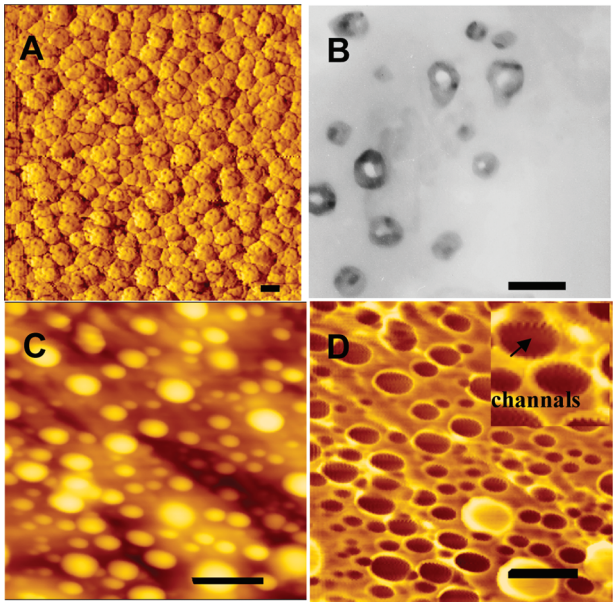

FIGURE 4. Morphology of the HPC−PAA nanoparticles and PAA nanogels in an aqueous medium with pH = 6.5. (A) AFM phase image of the HPC−PAA nanoparticles; (B) TEM image of the PAA nanogels; (C and D) AFM height and phase images of the PAA nanogels, respectively. The inset is the magnification image of individual PAA nanogels in part D. The scale bars are all 200 nm.

does not significantly increase, implying that the density of the nanogel increases greatly, which means that hollow nanogels have possibly turned into solid nanoparticles because of occupation of BSA macromolecules in the PAA nanogels. The TEM image (inset of Figure 5A) of the PAA nanogels after BSA loading confirms their solid structure, which indicates clearly that the hollow part of the nanogel has been occupied by the BSA molecules.

Table 1. Size and Scattering Intensity of the PAA Nanogels before and after Loading

	particle diameter (nm)	ζ potential (mV)	polydispersity	count rate (Kcps)
PAA gel (pH = 4.0)	206 ± 13	−1.5 ± 5	0.135	171.1
PAA gel (pH = 5.0)	214 ± 8	−20.3 ± 2	0.102	160.4
PAA gel (pH = 6.0)	238 ± 10	−51 ± 3	0.060	157.6
PAA−BSA gel (pH = 4.0)	198 ± 12	−19.3 ± 1	0.136	1300
PAA−BSA gel (pH = 5.0)	205 ± 10	−20.5 ± 2	0.098	1400
PAA−BSA gel (pH = 6.0)	216 ± 18	−26.3 ± 1	0.183	1500

As previously reported (29), the incubation process usually exhibited lower loading capacity compared to the encapsulation method. However, the PAA nanogels show superhigh loading capacity using the incubation method. The driving force of this process generally included coulombic (electrostatic) and hydrophobic interactions. To understand the key factor for the BSA loading, we investigated the loading capacity of the PAA nanogels in diverse initial concentrations of a BSA solution (0.2, 0.4, 0.6, 0.8, 1.0, 2.0, 3.0, 4.0, and 5.0 mg/mL) at pH = 4.0, 5.0, and 6.0, respectively. As far as the protein BSA is concerned here, its isoelectric point (IEP) is 4.9 (26); therefore, BSA possesses positive, zero, and negative charges when the pH is 4.0, 5.0, and 6.0, respectively. On the other hand, the surface charge of the PAA nanogels does not change and carried negative charges at these three pH values (Table 1). As a consequence, the electrostatic interaction between BSA molecules and PAA nanogels can be estimated by changing the pH of the system. From Figure 5A, it can be seen that the loading capacity increases with the BSA initial concentrations in all cases, and no obvious increase in loading is observed with a BSA concentration greater than 1 mg/mL, suggesting that the PAA nanogels have loaded BSA with saturation at this threshold. The highest amount for BSA loaded on the PAA nanogels is 8.0 mg/mg, which occurs at pH = 5.0, which is similar to the results reported in other porous materials in which the maximum BSA adsorption takes place near the IEP (30, 31). This behavior can be explained by the fact that, near the IEP, BSA has been close to zero charge and tends to show a minimum in solubility, leading to aggregates on the PAA nanogels. Hence, the loading capacity of this process is determined by hydrophobic interactions. When the pH of the system drops to 4.0, electrostatic attraction between BSA molecules and PAA nanogels occurs as a result of their opposite charges. In this case, both electrostatic and hydrophobic interactions influence the loading amount. In the case of pH = 6.0, both BSA and the PAA nanogel have

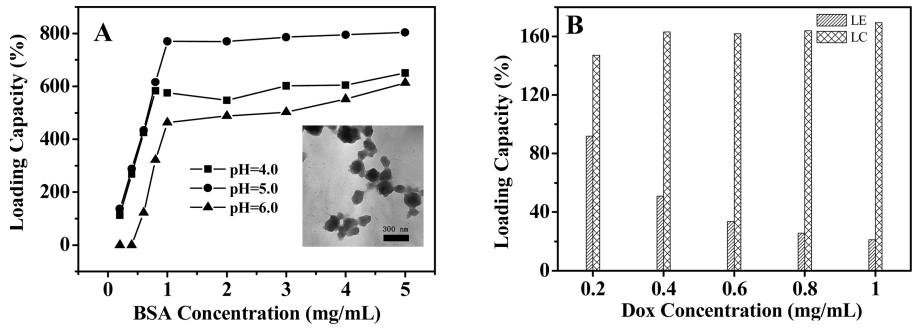

FIGURE 5. (A) Loading capacity of the PAA nanogel (0.125 mg/mL) in a BSA solution with diverse initial concentrations (0.2, 0.4, 0.6, 0.8, 1.0, 2.0, 3.0, 4.0, and 5.0 mg/mL) at pH = 4.0, 5.0, and 6.0. The inset is the TEM image of the PAA nanogels after BSA loading. The scale bar is 300 nm. (B) Loading capacity (LC) and loading efficiency (LE) of the PAA nanogels in a Dox solution at pH = 6.0.

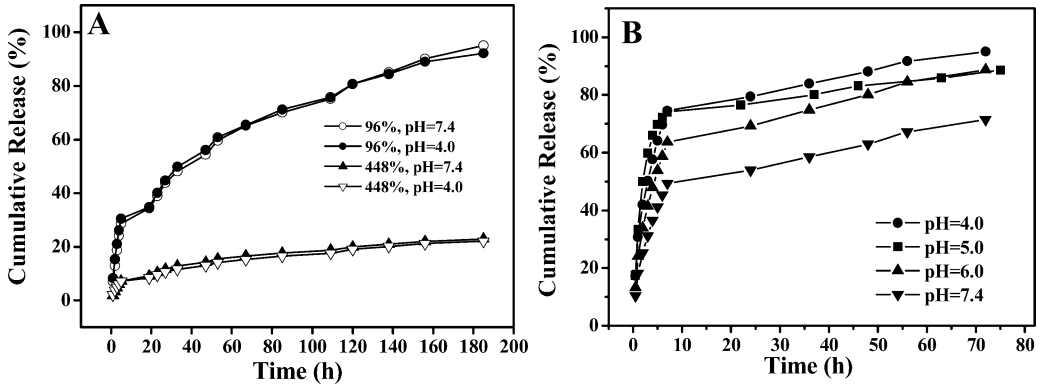

FIGURE 6. (A) Profile of BSA release from the PAA nanogels with different loading capacities at pH = 4.0 and 7.4 PBS solutions. (B) Profile of Dox release from the PAA nanogels in various pH media.

negative charges. Thus, the driving force of loading BSA onto the PAA nanogel becomes merely a hydrophobic interaction. The loading amount at this pH is less than that of pH = 4.0 because of electrostatic repulsion between BSA and the PAA nanogel. Nevertheless, PAA nanogels still exhibit a remarkably higher loading capacity of BSA compared to the usual protein carriers in despite of electrostatic repulsion at pH = 6.0. Hence, we deduce that electrostatic interaction is not the key driving force for BSA adsorption but hydrophobic interaction is. As for no loading at the initial two concentrations (0.2 and 0.4 mg/mL) when pH = 6.0, it can be explained that hydrophobic interaction at this medium pH is relatively weak at lower concentration. Besides hydrophobic interaction, the hollow core−porous shell structure of the PAA nanogels has crucial effects on the high-capacity adsorption process for two reasons. First, there are plenty of pores on the external surface of the PAA nanogels, which offer entrance channels for BSA to the cavity of the nanogels and make full use of the internal hollow structure. Thus, BSA could go through the porous shell into the cavity with high efficiency. Second, the size of pores may exactly match the size of the BSA molecules so that BSA could not drop out the PAA nanogels easily once they enter into the cavity. On the other hand, PAA nanogels form swollen cross-linked networks dispersed in solution and the nanosized spherical matrix should also play an important role in trapping and keeping of BSA. On the basis of the above discussion, it can be concluded that a porous hollow structure has a direct relationship with the high loading capacity of the PAA nanogels.

Because of the structural characteristics of the hollow porous PAA nanogel, it is also a good carrier for small molecular drugs. We choose an antitumor agent, Doxorubicin (Dox), as the model drug to investigate the loading capacity in PAA nanogels. We find that the highest loading capacity of Dox in the PAA nanogels reaches 169% (1.69 mg of Dox/mg of nanogel; Figure 5B) when the Dox concentration is above 1 mg/mL and the medium is at pH = 6.0. This is about 10 times higher than that for other analogous Dox-loaded systems (32). Because the pore size on the surface is too large in comparison with the size of Dox, Dox molecules can easily enter and escape from the nanogels. The loading capacity of Dox cannot reach the value above 200%, which is determined by the equilibrium based on the ionic interaction between Dox and PAA because Dox has a positive charge while PAA has negative charge at pH = 6.0.

Release Behavior of the PAA Nanogels. Besides drug loading, drug release is another important parameter for drug efficacy (33). Figure 6 shows the release profiles of BSA and Dox from the PAA nanogel in different pH environments at 37 °C. The release of BSA from the PAA nanogel is much slower, and no burst release is observed. It is apparent that the pH value of the release medium has little influence on the release behavior. Considering the high cross-linking degree of the PAA nanogels due to the large amount of cross-linker used to cross-link PAA, the pore size of the PAA nanogel should not change much with pH variation. Thus, a possible explanation of the release behavior is as follows:

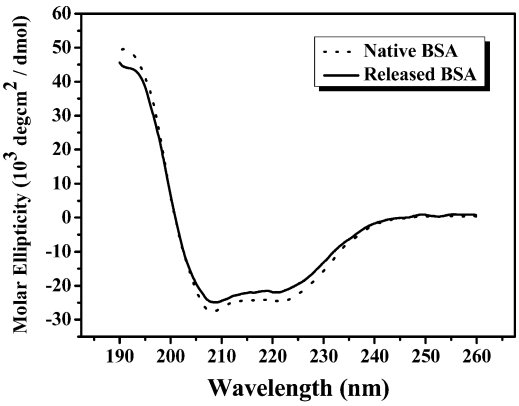

FIGURE 7. CD spectra of BSA: (A) native BSA; (B) BSA released from the PAA nanogels in a pH = 7.4 PBS solution.

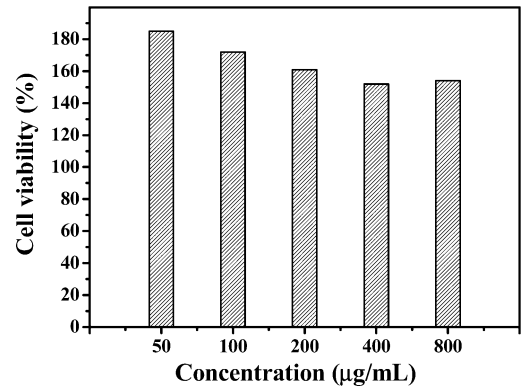

FIGURE 8. In vitro cytotoxicity of empty PAA nanogels against the LoVo cell line at normal concentration.

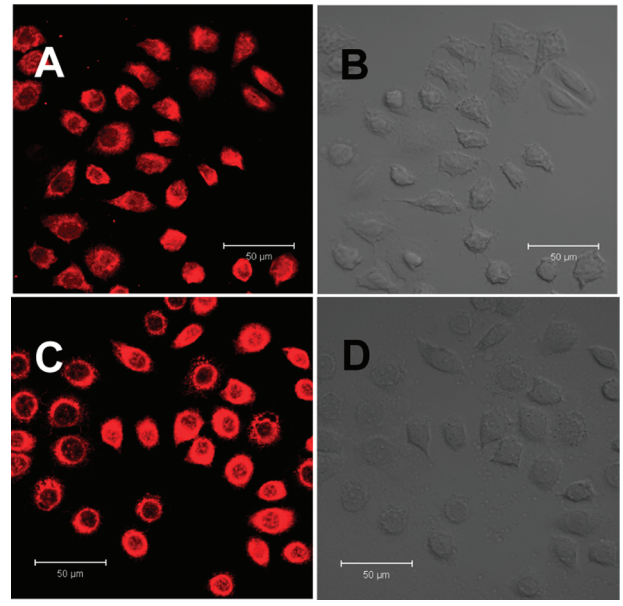

FIGURE 9. LCSM (left) and differential interference contrast (right) images of BCG 823 cells after incubation with RBITC-BSA-loaded (A and B) and Dox-loaded (C and D) PAA nanogels.

The dominating strength of the binding of the BSA in the nanogels is hydrophobic interaction; thus, the release process is just a combination of desorption and the diffusion process and is independent of the pH of the system. Second, loaded BSA is confined in the cavity of the PAA nanogel and surrounded by a porous polymer shell, and hereby sustained release is induced by slow diffusion through the nanogel matrix barrier layer.

In order to know if there is a structure change of BSA after loading and release, CD measurement was carried out, as shown in Figure 7. From CD spectra of native BSA and released BSA, it is indicated that the released BSA remains its original active structure. On the other hand, Dox could be released in response to the environmental changes; for example, the decrease in the pH value of the system speeds the release of BSA from the nanogel (Figure 6B), which is primarily ascribed to electrostatic interaction between the PAA chain and Dox. When PAA and Dox show opposite charges (pH = 7.4), electrostatic interaction between them would inhibit Dox release from the PAA nanogels. As the pH is decreased, the PAA nanogels gradually approach zero charge (pH = 4.0; the ζ potential is -1.5 mV), electrostatic interaction would weaken slowly, and Dox could go through the PAA nanogel matrix easily. Hence, the cumulative release amount of Dox from the PAA nanogels at pH = 4.0 is rather greater than that at pH = 7.4 (Figure 6B).

Cytotoxicity and Cellular Uptake of the PAA Nanogels. The cytotoxicity of the PAA nanogels was also investigated. It is found that there is no cytotoxicity for empty PAA nanogels in the test concentration range (Figure 8). To investigate the intracellular drug delivery of the PAA nanogels, the cellular uptake values of RBITC-BSA- and Dox-loaded PAA nanogels were examined using LCSM, respectively. As shown in Figure 9, a strong red fluorescent signal arising from RBTIC-labeled BSA or Dox itself is observed in the cell cytoplasm for both RBITC-BSA- and Dox-loaded PAA nanogels, indicating that the PAA nanogel can overcome cellular barriers to enter the intracelluar region, although it carries negative surface charges, which is consistent with the results reported by Savic et al. (34). High cellular uptake of negatively charged nanoparticles has been reported in some studies because there are some cationic domains in plasma membranes (35–38). It has been reported that the optimal nanoparticle size, cationic sites on the plasma membrane, and bending of the plasma membrane after adsorption of negatively charged particles at those cationic sites may contribute to the cellular uptake of negatively charged small particles. Therefore, we speculate that the PAA nanogels in this study might be taken up by the cells via a similar mechanism. This result indicates that the PAA nanogel may be a good carrier for drug delivery to the cell.

CONCLUSION

In this study, we have synthesized a novel hollow core–porous shell structure PAA nanogel by removal of HPC from cross-linked HPC–PAA nanoparticles. It was found that the nanogels have a hollow structure and are responsive to changes of the environmental pH. The nanogel exhibits a surprisingly high loading ability to both proteins and small molecular drugs, the loading capacity of which is at least 10 times higher than that of common drug carriers. The key driving force of BSA loading is hydrophobic interaction between protein and nanogels. The porous hollow structure

also plays an important role for the superhigh capacity of drugs. The PAA nanogels have also shown sustained drug release properties and can across biological barriers to deliver their payload inside the cells. Considering the high stability of the materials, simple and mild preparation procedure, high loading capacity, sustained-release property, and ability to protect biological agents from denaturation, PAA nanogels have a promising future as DDSs.

Acknowledgment. This work is supported by the Natural Science Foundation of China (Grants 50625311 and 20874042), the New Drug Preparation Program of MOST (Grant 2009ZX09503-028), and the Cultivation Fund of the Key Scientific and Technical Innovation Project, Ministry of Education of China (Grant 707028).

REFERENCES AND NOTES

(1) Vinogradov, S. V. In *Structure and Functional Properties of Colloidal Systems*; Hidalgo, A. R., Ed.; CRC Press: Boca Raton, FL, 2009; p 367.
(2) Rajendran, L.; Knoler, H. J.; Simons, K. *Nat. Rev. Drug Discovery* **2010**, *9*, 29.
(3) Puneet, U.; Subheet, J.; Tiwary, K. *Curr. Drug Delivery* **2010**, *7*, 152.
(4) Kim, S.; Shi, Y.; Kim, J. Y.; Park, K.; Cheng, J. X. *Expert Opin. Drug Delivery* **2010**, *7*, 49.
(5) Yallapu, M. M.; Reddy, M. K.; Labhasetwar, V. In *Biomedical Applications of Nanotechnology*; Labhasetwar, V., Lwslie-Pelecky, D. L., Eds.; John Wiley & Sons, Inc.: New York, 2007; p 131.
(6) Raemdonck, K.; Demeester, J.; Desmedt, S. *Soft Matter* **2009**, *5*, 707.
(7) Ulanski, P.; Rosiak, J. M. In *Encyclopedia of Nanoscience and Nanotechnology*; Nalwa, H. S., Ed.; American Scientific Publishers: Valencia, CA, 2004; p 845.
(8) Lee, E. S.; Kim, D.; Youn, Y. S.; Oh, K. T.; Bae, Y. H. *Angew. Chem., Int. Ed.* **2008**, *47*, 2418.
(9) Peppas, N. A.; Hilt, J. Z.; Khademhosseini, A.; Langer, R. *Adv. Mater.* **2006**, *18*, 1345.
(10) Zhu, Y.; Shi, J.; Shen, W.; Dong, X.; Feng, J.; Ruan, M.; Li, Y. *Angew. Chem., Int. Ed.* **2005**, *44*, 5083.
(11) Camargo, P. H.; Li, Z. Y.; Xia, Y. *Soft Matter* **2007**, *3*, 1215.
(12) Chen, M.; Wu, L.; Zhou, S.; You, B. *Adv. Mater.* **2006**, *18*, 801.
(13) Kamata, K.; Lu, Y.; Xia, Y. *J. Am. Chem. Soc.* **2003**, *125*, 2384.
(14) Yin, Y.; Rioux, R. M.; Erdonmez, C. K.; Hughes, S.; Somorjai, G. A.; Alivisatos, A. P. *Science* **2004**, *304*, 711.
(15) Caruso, F.; Caruso, R. A.; Mohwald, H. *Science* **1998**, *282*, 1111.
(16) Feng, Z. G.; Li, Y. S.; Niu, D. C.; Li, L.; Zhao, W. R.; Chen, H. R.; Li, L.; Gao, J. H.; Ruan, M. L.; Shi, J. L. *Chem. Commun.* **2008**, 2629.
(17) Kim, J.; Kim, H. S.; Lee, N.; Kim, T.; Kim, H.; Yu, T.; Song, I. C.; Moon, W. K.; Hyeon, T. *Angew. Chem., Int. Ed.* **2008**, *47*, 8438.
(18) Zhang, T. R.; Ge, J. P.; Hu, Y. X.; Zhang, Q.; Aloni, S.; Yin, Y. D. *Angew.Chem., Int. Ed.* **2008**, *47*, 5806.
(19) Li, H. X.; Bian, Z. F.; Zhu, J.; Zhang, D. Q.; Li, G. S.; Huo, Y. N.; Li, H.; Lu, Y. F. *J. Am. Chem. Soc.* **2007**, *129*, 8406.
(20) Xie, B. Q.; Shi, H. F.; Liu, G. M.; Zhou, Y.; Wang, Y.; Zhao, Y.; Wang, D. J. *Chem. Mater.* **2008**, *20*, 3099.
(21) Chen, Y.; Ding, D.; Mao, Z.; He, Y.; Hu, Y.; Wu, W.; Jiang, X. *Biomacromolecules* **2008**, *9*, 2609.
(22) Hu, Z. B.; Xia, X. H. *Adv. Mater.* **2004**, *16*, 305.
(23) Khutoryanskiy, V. V.; Cascone, M. G.; Lazzeri, L.; Barbani, N.; Nurkeeva, Z. S.; Mun, G. A.; Dubolazov, A. V. *Polym. Int.* **2004**, *53*, 307.
(24) Li, Y.; Yang, H. H.; You, Q. H.; Zhuang, Z. X.; Wang, X. R. *Anal. Chem.* **2006**, *78*, 317.
(25) Bradford, M. M. *Anal. Biochem.* **1976**, *72*, 248.
(26) Raj, T.; Flygare, W. H. *Biochemistry* **1975**, *13*, 3336.
(27) Janes, K. A.; Calvo, P.; Alonso, M. J. *Adv. Drug Delivery Rev.* **2002**, *47*, 83.
(28) Cai, C. F.; Bakowsky, U.; Rytting, E.; Schaper, A. K.; Kissel, T. *Eur. J. Pharm. Biopharm.* **2008**, *69*, 31.
(29) Kabanov, A. V.; Vinogradov, S. V. *Angew. Chem., Int. Ed.* **2009**, *48*, 5418.
(30) Dillman, W. J.; Miller, I. F. *J. Colloid Interface Sci.* **1973**, *44*, 221.
(31) Chen, Y.; Wang, Y. J.; Yang, L. M.; Luo, G. S. *AIChE J.* **2007**, *53*, 298.
(32) Yan, E.; Ding, Y.; Chen, C.; Li, R.; Hu, Y.; Jiang, X. *Chem. Commun.* **2009**, 2178.
(33) Soppimath, K. S.; Aminabhavi, T. M.; Kulkarni, A. R.; Rudzinski, W. E. *J. Controlled Release* **2001**, *70*, 1.
(34) Savic, R.; Luo, L.; Eisenberg, A.; Maysinger, D. *Science* **2003**, *300*, 615.
(35) Wilhelm, C.; Billotey, C.; Roger, J.; Pons, J. N.; Bacri, J. C.; Gazeau, F. *Biomaterials* **2003**, *24*, 1001.
(36) Miller, C. R.; Bondurant, B.; Mclean, S. D.; McGovern, K. A.; O'Brien, D. F. *Biochemistry* **1998**, *37*, 12875.
(37) Patil, S.; Sandberg, A.; Heckert, E.; Self, W.; Seal, S. *Biomaterials* **2007**, *28*, 4600.
(38) Guo, R.; Li, R.; Li, X.; Zhang, L.; Jiang, X.; Liu, B. *Small* **2009**, *5*, 709.

AM100709D